Stochastic Approach for Feature-based Localization and Planning in Nano-manipulations

Shuai Yuan, Zhidong Wang, Lianqing Liu, Ning Xi, Yuechao Wang

Abstract — In AFM based nano-manipulation, the tip position uncertainties still exist due to the parameter inaccuracies in the open-loop compensation of the piezo scanner, the noise in the closed-loop control and thermal drift. These spatial uncertainties are very challengeable to be directly estimated owing to the lack of real time feedback, and its effects are more significant in performing an automatic nano-manipulation/assembly task than macro world manipulations. In this paper, we propose a stochastic framework for feature-based localization and planning in nano-manipulations to cope with these uncertainties. In the proposed framework, some features in the sample surface are identified to calculate their positions in statistics, and then detected by using the AFM tip as the sensor itself through a local-scan based motion. In the localization, the Kalman filter is used through incorporating the tip motion model and the local-scan based observation model to estimate the on-line tip position in the task space. The simulation and experiments about tip positioning are carried out to illustrate the validity and feasibility of the proposed algorithm. Finally, a carbon nanotube is followed to show that the proposed method can provide a great potential for improving the position accuracy.

Index Terms— AFM based Nano-manipulation, AFM Tip Localization, Feature based Localization, Kalman Filter.

I. Introduction

OBSERVATION and manipulation at nano-scale using Atomic Force Microscopy (AFM) as an executive robot have been developed for over a decade, and provide promising potential for manufacturing nanostructures and nano-devices [1-9]. The AFM uses the tip as an end effector of the robot to image the nano-objects with its high resolution and manipulate them with its high alignment precision [10]. The critical technology to achieve this manipulation is to accurately position the tip around the target objects. However, there are large uncertainties of the tip position due to the hysteresis, creep, and other nonlinearities of the piezoelectric scanners as well as the system thermal drift. These factors have extreme influences on the tip positioning at nano-scale. Therefore, it is full of challenge to effectively and accurately observe and manipulate the nano-objects based on AFM, for the tip position cannot be accurately guaranteed in the task space.

Spatial uncertainties are partially caused by the PZT scanner [11]. To reduce the hysteretic and creep effects of piezo material (PbZrTiO3: PZT), two types of methods are developed: sensor based closed-loop control and model based compensation. These methods can only improve the expanding and contracting accuracy between the tip and the PZT central axis. The tip position in the sample surface cannot be guaranteed because of thermal drift, which is caused by the contraction and expansion of AFM mechanical components due to temperature change, humidity change, etc[10,12]. Several methods [12, 15-17] are proposed to predict the thermal drift between the tip frame and the sample surface frame (task frame), and then indirectly estimating the tip position.

In contrast to abovementioned methods, the represented approach directly localizes the on-line tip position by intermittently observing the feature (landmark) in the sample surface (task frame), referring to the macro robotic localization [18]. And our previous work [19] has been done to estimate the tip position by using local scan based observation. Furthermore, the uncertainties of the landmark position and the tip motion due to the PZT scanner control need to be considered in the deeper research. The effects of these uncertainties are more significant in performing a nano-manipulation/assembly task than macro world manipulations, because the uncertainties are relatively large at the size of nano-objects and the scale of manipulation motion. In addition, sensors in AFM control system are only able to be equipped on the PZT or the cantilever of an AFM as a joint space sensor, and current technology cannot directly provide online sensing the tip position in the task space. This may bring further difficulty to perceive the tip position precisely in both tip motion control and nano-object manipulation. A *Stochastic Approach for Feature-based Localization and Planning* (SAFLP) is proposed in the paper. The main idea of this strategy is to incorporate a stochastic approach with a probabilistic filter based localization algorithm that is similar to SLAM algorithms for macro robot localization [20-21]. This algorithm is developed by combining observation data of perceiving a feature with the tip motion control input [22].

In this research, the tip position uncertainties are represented

Manuscript received March 20, 2016. This research work is partially supported by the National Natural Science Foundation of China (Project Codes: 61175103, 61305125), National Post Doctor Foundation (Project Codes: 2013M530955, 2014T70265)), The National 863 project (2012AA020100) and Chinese Academy of Sciences State Foreign Expert Bureau International Partnership Program for Creative Research Teams.

S. Yuan, L.Q. Liu, Y.C. Wang are with the State Key Laboratory of Robotics, Shenyang Institute of Automation, Chinese Academy of Sciences, Shenyang, Liaoning Province 110016, China. S. Yuan is with the school of Information & Control Engineering, Shenyang Jianzhu University, Shenyang, Liaoning Province 110168, China, and also is with the graduate school of Chinese Academy of Sciences, Beijing 100001, China.
(Email: yuanshuai @sia.cn; lianqingliu@sia.cn).

Z.D. Wang is with Department of Advanced Robotics, Chiba Institute of Technology, Chiba, 275-0016, JAPAN. (Email: zhidong.wang@it-chiba.ac.jp).

N. Xi is with Department of Electrical and Computer Engineering, Michigan State University, East Lansing, MI 48823 USA. (Email: xin@msu.edu).

by probability distribution. The feature based observation is developed to correct the tip position with higher accuracy [23] by using local scan. A nano-particle is typically selected as a feature to build an observation model. Upon observing the nano-particle, the tip position is optimally updated by combining with the tip motion control input. In this paper, many experiments are included to estimate the probabilistic parameters of the tip motion model and the observation model. Then simulations and corresponding experimental results are represented to illustrate the validity of the proposed method. Finally, a carbon nanotube is followed to show that the proposed method can provide a great potential for improving the position accuracy.

The structure of this paper is arranged as follows. A general framework of the tip position updating algorithm is given in Section II. In Section III, the stochastic feature-based observation model based on local scan is proposed. The simulation and SAFLP based localization experiments results are introduced in Section IV. Positioning accuracy is further discussed through following carbon nanotube in section V. Section VI are conclusion and the future work.

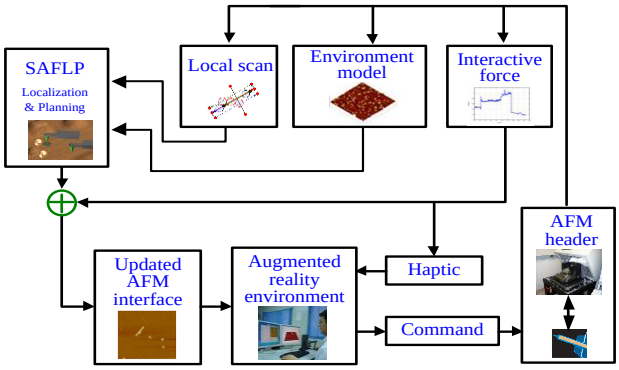

Fig.1. Architecture of AFM based nano-manipulation system by using stochastic approach for feature-based localization and planning

II. The Proposed Framework of SAFLP

In recent years, many kinds of AFM Based nano-manipulation systems[4-7],[10-11],[24-31] have been developed to perform manipulation. The force model based AFM nano-manipulation [4] is proposed to continuously push the nano-particle until that the particle is maneuvered to the target position, by monitoring the contact status between the tip and the nano-particle. The method in [24] performs image scan and nano-manipulation in parallel through the collaboration of two cantilevers: one cantilever acts as an imaging sensor and the other is used as a manipulating tool. Those works do not consider the importance of the tip position accuracy related to the maneuvered object. For reducing the spatial uncertainties, this paper proposes a new framework of stochastic approach for the AFM based manipulation (Fig.1). The tip in the task frame is used as an observer sensing itself position as well as a manipulation effector. This sensing procedure couples the tip observation with its motion, and is not similar to the macro robot performing detection using outer sensors. The tip position is estimated by using Kalman filter in the observation procedure coupled with the tip motion, and this procedure widely exists in the 'touch' mode application such as scanning probe microscopy, and force tactile sensing instrument.

During nano-manipulations, the AFM tip is usually used to push the nano-objects to their target positions. Fig.2 (a) shows an example of nano-assembly task in which a nano-rod is moved to bridge the two electrodes for building a nano-device. As the various uncertainties exist in the nano-environments, the tip position can be described with the probability distribution. This distribution will become larger with the tip moving and time increasing. Fig.2 (b) shows that the uncertainty of tip position will increase larger when it is moved to the position for pushing the nano-rod. Since the AFM tip can only apply force through contact point, the uncertainty of the pushing point will lead to larger uncertainties of the position and orientation of the pushed nano-object. As the result, the nano-rod may not correctively bridge the two electrodes, and the AFM needs to repeat scanning and nano-rod pushing. This is considered as a main reason that current nano-assemblies cannot be applied in the factory automation.

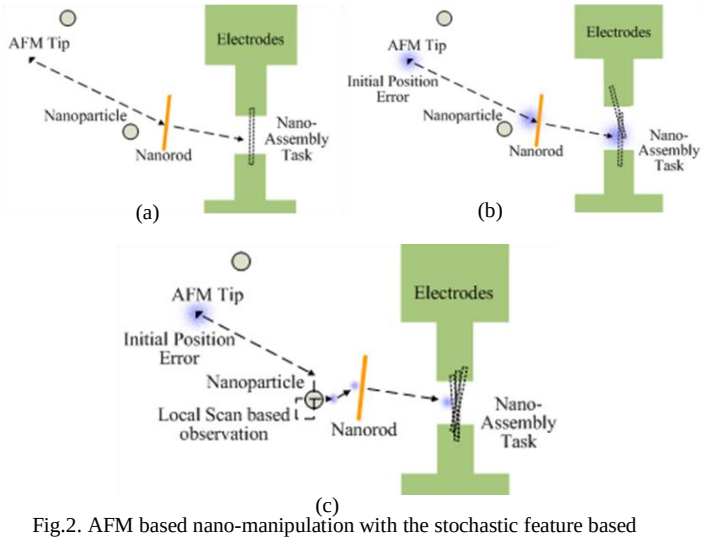

Fig.2. AFM based nano-manipulation with the stochastic feature based localization and planning

For reducing and limiting the spatial uncertainties of the tip at the target position under a predefined allowance, a trajectory of the AFM tip is planned as follows (see Fig.2 (c)). First, a feature near the target position for pushing nano-object is selected and the tip is moved around it. Then the local-scan actions on two perpendicular directions are performed for observing the feature position and the tip position is updated stochastically. By using the updated position with higher accuracy, the tip is moved to the target position for pushing the nano-rod to bridge the electrodes. This maneuver will lead to a higher success rate of nano-assembly.

The new architecture is considered in the SAFLP including a kind of feedback control on the AFM tip motion during nano-manipulations (Fig.3). It should be emphasized that the SAFLP architecture has two very different points from general feedback control systems. The first point is that two types of data are incorporated in the feedback loop: the motion estimation data and the observation data based on local scan. The feedback loop associated with tip position estimation by using motion model is executed in high sampling frequency, but the uncertainty of the tip position distribution will increase,

because the uncertainties of the estimation are accumulating. On the other hand, the feedback loop associated with observing features in the task space and updating position by using probabilistic filter will improve the estimation accuracy. This updating process can only be executed in a very low frequency, because it is based on the local scan actions. The second point is that a probabilistic trajectory planner is included into the control loop for planning one or more local scan motions before a motion to the final target. This is a key component for realizing the tip position control under a desired allowance at the target position.

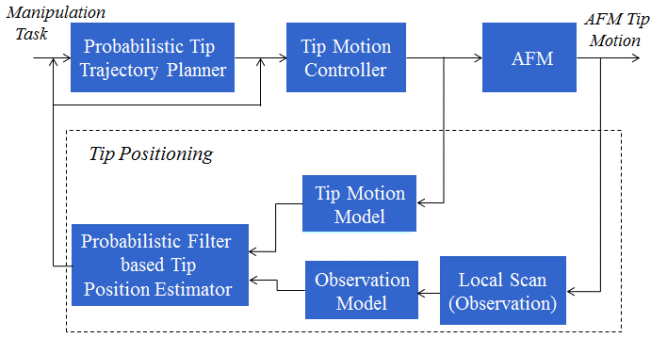

Fig.3. The architecture of stochastic feature based localization and planning

III. Feature and Local Scan Based Observation

The spatial uncertainty of the AFM tip is increasing with the tip motion. In order to reduce the uncertainty, the center of the nano-particle is intermittently observed to estimate the tip observation position at the nano-particle center by using the Kalman filter. Then the tip current position relative to the center of the nano-particle is calculated according to the motion model. Finally, the tip position is estimated in the task frame.

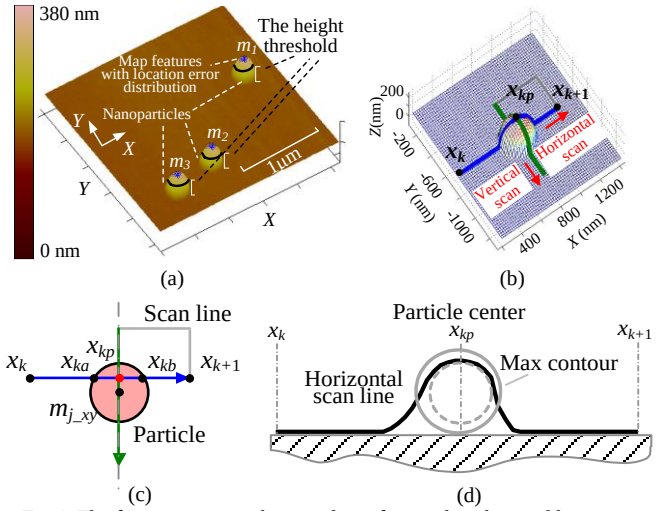

Fig.4. The feature exists in the sample surface and is observed by using local scan trajectory. (a)The location of features is calculated in the priori imaging map. (b) The tip trajectory is planned for observing landmark in 3D. (c) The landmark location is estimated by using local scan trajectory including the first horizontal scan and the second vertical scan. The first scan cross the nanoparticle bounder at x_{ka} and x_{kb}, then their center x_{kp} is calculated for determining vertical scan to estimate nanoparticle center m_{j_xy}. (d) Horizontal scan profile is shown.

A. Maps and Stochastic Feature Definitions

The AFM tip perceives features in the nano-manipulation region. M denotes features such as nano-particles, nano-rods, etc. in the target region map. m describes the location of a feature, and N is the total number of features in the region.

$$M_N = \{m_1, m_2, m_3, ..., m_N\} \quad (1)$$

Expression 1 shows the stochastic feature map generated from the image of nano-manipulation region.

$$m_j = m_{j,xy} + v_{map} \qquad v_{map} \sim N(0, Q_{map}) \quad (2)$$

where $m_{j,xy}$ is a two dimension vector expressing the center position of the particle j in the image frame. It can be obtained by calculating the center of the cluster of the pixels in the scanning image (see Fig.4(a)), and these pixels are higher than a predefined height threshold. v_{map} is an error random variable with zero mean Gaussian distribution Q_{map}. This error variable mainly depends on the errors from scanning motion, such as effect of thermal drift, and the errors from imaging procedure, and the uncertainties caused by image resolution limitation. Its distribution can be calibrated by processing multiple scanning images of the same particle, as introduced in [23]

B. Local Scan Based Observation

Feature observation during nano-manipulation is performed by using a local scan including a horizontal scan and a vertical scan shown in Fig.4 (a) and (b). Fig.4(c) shows that the nanoparticle center x_{kp} in horizontal scan is calculated by using x_{ka} and x_{kb}, and then nanoparticle center m_{j_xy} is obtained similarly in the vertical scan. Fig.4(d) shows that the horizontal observation during a local scan period from x_k to x_{k+1} will be defined as obtaining the nano-particle center x_{kp} in a scan profile.

The observation process is analyzed in detail (see Fig.5). The whole scan profile can be divided into two parts: first, scan profile 1 from x_k to x_{kp} , second, scan profile 2 from x_{kp} to x_{k+1}. The tip posterior distribution $\hat{x}(kp \mid kp)$ at x_{kp} is estimated by using the Kalman filter through combining the motion control $\hat{x}(kp \mid k)$ with the observation data $h'(x_{kp}, m_j)$ .Then the tip position belief $\hat{x}(k+1 \mid k+1)$ at x_{k+1} is calculated according to the motion control u_{kp} from x_{kp} to x_{k+1}.

In comparison with the macro robot localization in the physical world, the local scan based observational strategy possesses two important characteristics:

First, the macro robot observation is achieved through the position sensor onsite, therefore the macro observation does not rely on the motion. Since the observation in the study depends on the tip motion path, this characteristic is distinct from the macro robot localization.

Second, when observing the feature, SALFP does not update the tip distribution at x_{k+1} directly, but the observation position x_{kp}. Then the current distribution at x_{k+1} after x_{kp} is estimated according to the motion model.

In general, z_k is associated with information of tip position x_k and the feature j in the map. However, the nano-observation is different from the general sensing that occur at a certain position, and it is associated with a path from previous tip position x_k to the current tip position x_{k+1} for locally scanning

the nano-particle, and the measurement z_{kp} at the observation position is defined as follows:

$$z_{kp} = h(x_k, x_{k+1}, m_j) + v_{z,kp} \qquad v_{z,kp} \sim N(0, Q_{z,kp}) \tag{3}$$

where, $h(*,*,*)$ is the observation function and $v_{z,kp}$ is the error variable from measurement. Without losing generality, we can assume that the AFM tip takes exactly one measurement at each local scan, because it is possible to select a feature particle which is adjacent to other features. Thus the sequence of measurements is:

$$Z_k = \{z_0, z_1, z_2, ..., z_k\} \tag{4}$$

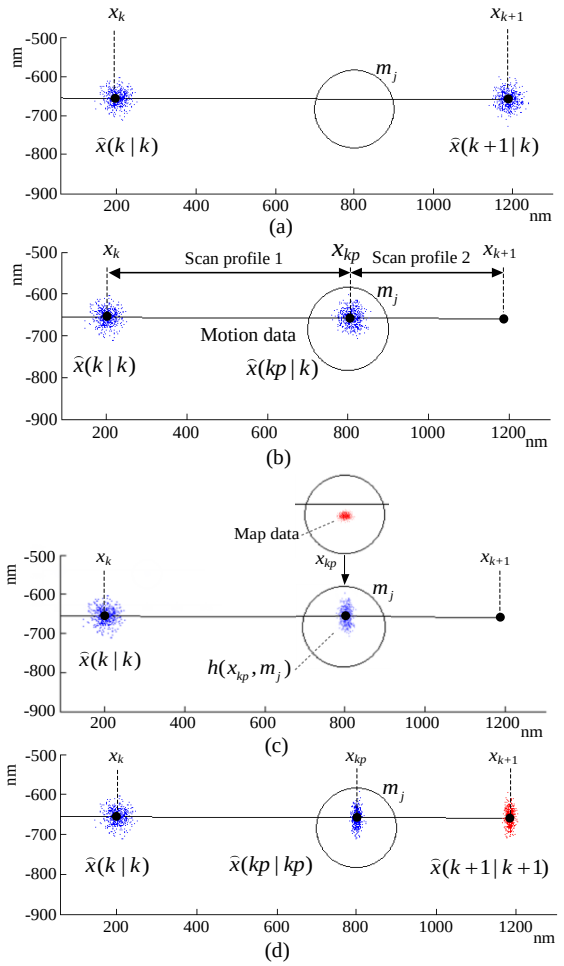

Fig.5. The tip distribution is updated during local scan based observation. (a) The tip scans frm x_k to x_{k+1}. (b) The nanoparticle center $x(kp|k)$ in the horizontal direction is estimated by using Eq.5 and Eq.6 according to the motion model. (c) The observation data is obtained from m_j in the map. (d) Finally, the nanoparticle center $x(kp|k)$ is calculated by using motion value $x(kp|kp)$and observation value z_{kp} according to Kalman Eq.7-Eq.15.

A scan trajectory can be obtained when the AFM tip performs a scan across the particle in Fig.5. The tip predictable position $x(kp|k)$ at nano-particle center on the scan profile is calculated by:

$$\hat{x}(kp|k) = x_k + l_{k1}^* \frac{x_{k,kp}^*}{\|x_{k,kp}^*\|} + w_{kp} \qquad w_{kp} \sim N(0, R_{kp}) \tag{5}$$

where l_{k1} is a scalar variable denoting scan length (tip motion control) from x_k to x_{kp} in the scan profile in Fig.5, l_{k1}^* is the mean of l_{k1}, $x_{k,kp}$ is a random variable vector from x_k to x_{kp}, and $\| x_{k,kp}^* \|$ is the norm of the mean value of $x_{k,kp}$, i.e. l_{k1}. $x_{k,kp}^* / \| x_{k,kp}^* \|$ denotes the unit vector in the direction of the local scan in the task frame. w_{kp} is an error random variable that is the linear superposition of error random variables w_k from the tip position at x_k and w_{k1} from tip motion control between x_k and x_{kp}.

For accurately calculating x_{kp}, l_{kp} can be computed as the middle point of x_{ka} and x_{kb} that are two intersection points between the scan trajectory and the line of height threshold (see Fig.5) defined to search the clustered pixels of the particles in the image. In general, this computation has stable result comparing with finding highest point directly from the height scan profile, because small height error near x_{kp} may lead to the big changes of the highest point position. l_{k1} is calculated as follows:

$$\begin{aligned} l_{k1} &= \frac{1}{2}(x_{ka} + x_{kb}) + \quad w_{k1} & w_{k1} &\sim N(0, R_{k1}) \\ w_{kp} &= w_k + w_{k1} & w_{kp} &\sim N(0, R_{kp}) \\ w_{k1} &= \frac{1}{2}(w_{ka} + w_{kb} + r_{ka} + r_{kb}) \end{aligned} \tag{6}$$

where, w_{ka} and w_{kb} are error random variables of tip motions from x_k to x_{ka}, and to x_{kb} respectively in the scan frame. r_{ka} and r_{kb} are error random variables from calculating two intersection points x_{ka} and x_{kb} respectively. Since the observation at time kp is practically performed for obtaining the tip distribution at x_{kp}.

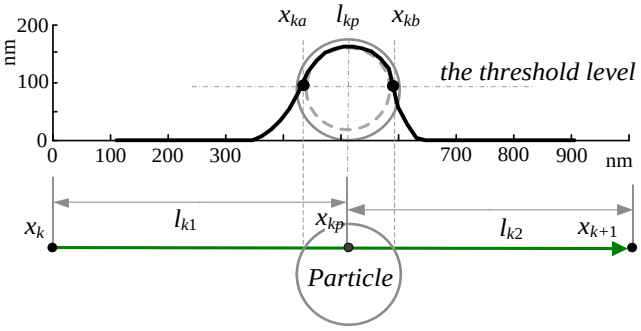

Fig.6. Observation model based on the scanning line

Eq.3 can be given by:

$$z_{kp} = h(x_{kp}, m_j) + v_{z,kp} \qquad v_{z,kp} \sim N(0, Q_{z,kp}) \tag{7}$$

To use the Kalman filter to localize the tip position, the observation function can be derived by:

$$h(x_{kp}, m_j) = x(kp|k) \tag{8}$$

while the observation data is actually obtained by assuming that the nano-particle center (x_{kp}) of the scan profile has the same weight value of the particle center ($m_{j,xy}$) in the local scan direction. Then the observation formula can be defined as following:

$$h'(x_{kp}, m_j) = R_\theta^T (S_x R_\theta m_{j,xy} + S_y R_\theta x_{kp}) \tag{9}$$

where $R_\theta \in R^{2\times 2}$ is the rotational matrix of local scan direction, S_x and S_y are selection matrixes:

$$S_x = \begin{pmatrix} 1 & 0 \\ 0 & 0 \end{pmatrix}, \quad S_y = \begin{pmatrix} 0 & 0 \\ 0 & 1 \end{pmatrix} \tag{10}$$

It is easy to know that a local scan action only provides one-dimension observation and two non-parallel local scan

actions are requested to have a full observation of two-dimension position information in the task fame. In general, we simply design these two local-scan directions as horizontal and vertical direction in task frame. This is convenient for setting motion commands, and also simplifying the observation calculation function, for the rotational matrix R_θ is simply.

The uncertainties of local scan based observation mainly consists of three parts of error sources that are independent mutually: errors in the map (v_{map}), errors of the different nano-particle centers in various local scan lines (v_{z_kl}) and errors from local scan direction deviation (v_{z_θ}). The combined random variable for these three errors is the linear superposition as follow:

$$v_{z,kp} = v_{map} + v_{z\_kl} + v_{z\_\theta} \tag{11}$$

C. Tip Position Estimation Based on the Kalman Filter

The Kalman filter is used to estimate the tip optimal position based on the tip motion model and the feature measurement model.

Given the tip motion control $u(k)$, AFM tip position is estimated at the nano-particle center x_{kp}. The prediction of the tip position based on the motion model is expressed by:

$$\begin{aligned} \hat{x}(kp \mid k) &= g(\hat{x}(k \mid k), u(k)) \\ P(kp \mid k) &= \nabla g\, P(k \mid k) \nabla g^T + R(kp) \end{aligned} \tag{12}$$

P is the covariance matrix of state x. If tip motion is not associated with local scan, there is no observation being performed and current estimation result $\hat{x}(k+1 \mid k)$ will be used as the state $\hat{x}(k+1 \mid k+1)$.

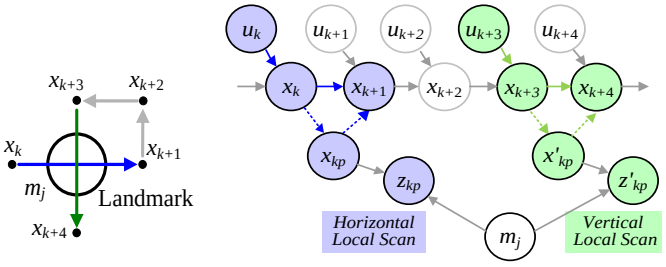

(a) Local scan path (b) Graphical model of tip positioning

Fig.7. Scan path and graphical model of tip positioning by two independent local scans. m indicates landmark, x_k at time k indicates the tip position, u_k indicates the motion control, and z_k indicates the measurement.

A full local-scan consists of four steps, which includes two one-dimension observations on scanning a landmark in perpendicular direction (see Fig.7). The Kalman filter based estimation based on observation and match is described as follows:

$$\begin{aligned} \hat{z}_i(kp) &= h(\hat{x}(kp \mid k), m_j) \qquad i = 1, \ldots, N \\ v_{ij}(kp) &= \left[z_j(kp) - \hat{z}_i(kp) \right] \\ &= \left[z_j(kp) - h(\hat{x}(kp \mid k), m_j) \right] \end{aligned} \tag{13}$$

$$\begin{aligned} S_{ij}(kp) &= E\left[v_{ij}(kp) v_{ij}^K(kp) \right] \\ &= \nabla h\, P(kp \mid k) \nabla h^K + Q_j(kp) \end{aligned} \tag{14}$$

where S is the covariance matrix for local scan based observation. By applying the corresponding check condition: $v_{ij}(kp) S_{ij}^{-1}(kp) v_{ij}^K(kp) \le g^2$, the associated feature particle will be identified. Then the tip position estimation is performed as follows:

$$\begin{aligned} W(kp) &= P(kp \mid k)\, \nabla h^K S_{ij}^{-1}(kp) \\ \hat{x}(kp \mid kp) &= \hat{x}(kp \mid k) + W(kp) v(kp) \\ P(kp \mid kp) &= P(kp \mid k) - W(kp) S(kp) W^K(kp) \end{aligned} \tag{15}$$

Once the position at x_{kp} is calculated, its position at x_{k+1} and its covariance is estimated by:

$$\begin{aligned} x_{k+1} &= x_{kp} + u_{kp} \\ P(x_{k+1}) &= P(x_{kp}) + R_{k+1} \end{aligned} \tag{16}$$

IV. Implementation and Experimental Results

The motion and observation models are incorporated to estimate the tip position by using the Kalman filter. The parameters for these models are calibrated through designed experiments or referring to the manuals. These model parameters of motion and observation are calibrated for the PZT without sensor based control. Then the algorithm is verified by simulation and the corresponding experimental results.

To illustrate the validity of the proposed algorithm, the following simulation and experiment are designed, and performed with veeco Dimension 3100. The parameters of motion model and observation model are calibrated by using the abovementioned methods.

Fig.8 shows a simulation procedure of a tip motion control from a start position x_0 to a target position x_8. Assuming the tip initial distribution is at x_0, if the tip is moved to x_8 directly without observing the feature by path $x_0 \rightarrow x_{d\_1} \rightarrow x_8$ marked by dash line, then its position distribution at x_8 will go beyond the predefined allowance. For improving the accuracy of AFM tip position, a nano-particle near the target position is used as the feature for local-scan based observation and position estimation, and the path of the AFM tip motion is marked by solid line.

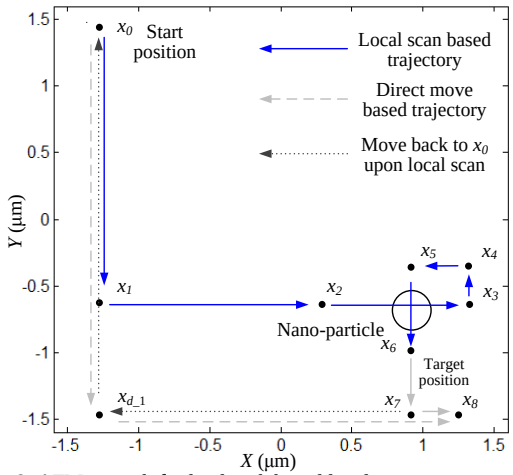

Fig.8. AFM tip path for landmark based localization experiments

In the direct move or SAFLP based experiments, the real AFM tip positions are recorded at x_0 and x_8 in common, and one waypoint (x_{d_1}) or three waypoints (x_2, x_5, x_6) respectively by punching small dents on the CD substrate surface. For the latter experiment, the tip position at x_6 is estimated by observing the

feature. Then the motion control input is calculated to move the tip to the target position x_8 for obtaining higher accuracy. In order to obtain probabilistic distribution of the abovementioned positions, a certain amount of experiments designed with the same tip motion pattern are needed to statistically count the distribution. Because the tip position distribution is relatively small, it is possible that two dents punched are overlapped partially or even fully if we do two or more experiments by using the same particle as the feature for localization. To obtain correct position results, all experiments are performed on different particles to avoid position overlapping of dents punched by the AFM tip.

In the experiments, multiple polystyrene nano-particles with the diameter about 200nm are scattered on the CD substrate. An area including at least one nano-particle is selected and pre-imaged. Then we stop imaging and move the tip to the center of the scanning region. Next, we need to move the tip to x_0 stochastically with the same distribution for each experiment. This procedure is realized by the following steps: first, moves the AFM tip from the center to x_2; second, performs local-scan based localization by path $x_2 \rightarrow x_3 \rightarrow \cdots \rightarrow x_6$; third, updates the tip position x_6, plans and moves the tip to x_8 with high accuracy by path $x_6 \rightarrow x_7 \rightarrow x_8$; Finally, moves to x_0 by path $x_8 \rightarrow x_{d\_1} \rightarrow x_0$ which is marked by dotted line in Fig.8 and punches the dent at x_0. Due to the long moving distance from x_8, the uncertainties of the tip position at x_0 will increase.

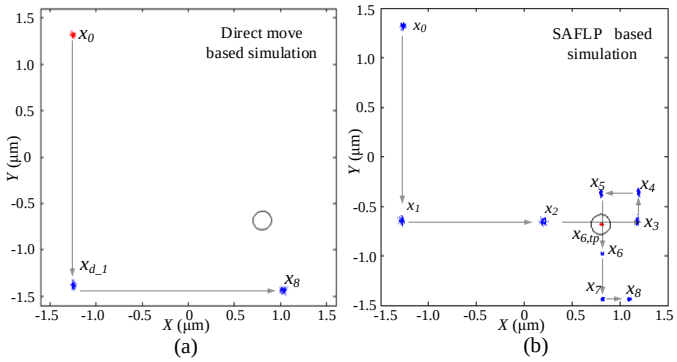

Fig.9. (a) Simulation result of moving the tip to its target position through direct moving without SAFLP algorithm. (b) Simulation result of moving the tip to its target position through local scan with SAFLP algorithm.

The simulation for direct move based experiments and SAFLP based experiments are performed, the distribution of tip position on waypoints are shown in Fig.9 (a) and (b). The uncertainty of the tip position at the target position is reduced significantly by applying SALFP approach.

These statistic experimental results illustrate the validity and the feasibility of SAFLP approach. At the same time, it should be noted that the standard deviation of the tip position at the target position is with the very similar values between simulation and the experiments. This result also illustrates that the calibration methods for motion model and observation models are valid.

Fifty of direct move based experiments have been performed, and the result of one experiment is shown in Fig.10. The center position of the nano-particle is set at the coordinate (0.801 μm, -0.684 μm). The punched dents can be observed inside the white dash line circles in Fig.10. Compared with direct move based experiment, fifty of SAFLP based experiments have been performed and one experiment result is shown in Fig.11. The punched dents inside the white dash line circles are used to mark the AFM tip positions.

Fifty of direct move based data sets and fifty of SAFLP based data sets are shown in Table 1 and Table 2 respectively. Both simulations and experiments use the same parameters of motion model and observation model calibrated by abovementioned experiments.

Table 1 shows that the standard deviation of the tip position distribution apparently increases to ~20 nm at x_8 with a long distance tip motion without using the SAFLP algorithm. Table 2 represents that after the local-scan based localization, uncertainty of tip position is effectively reduced to smaller distribution with standard deviation near and less than 6nm at x_6, and 9nm at x_8. As for other waypoints, the simulation results and experimental results in Table 1 and Table 2 are similar under one order of magnitude.

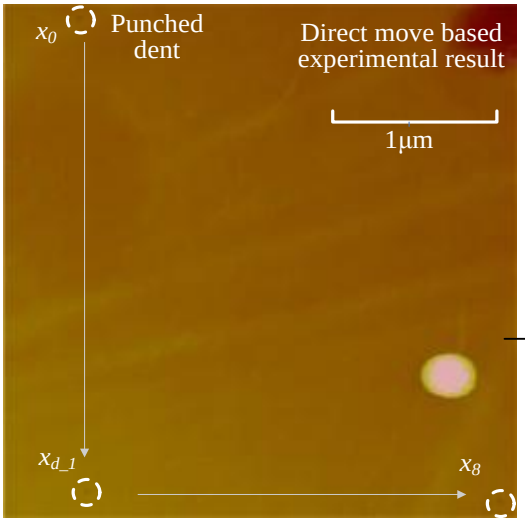

Fig.10. The tip is directly moved from x_0 to x_8. The tip positions at x_0, x_8 and the way point x_{d_1} are recorded by punching the indents. Scanning image shows that these punched indents observed in the white dash line circles marks the tip positions in the different way points. 50 experiments have been performed.

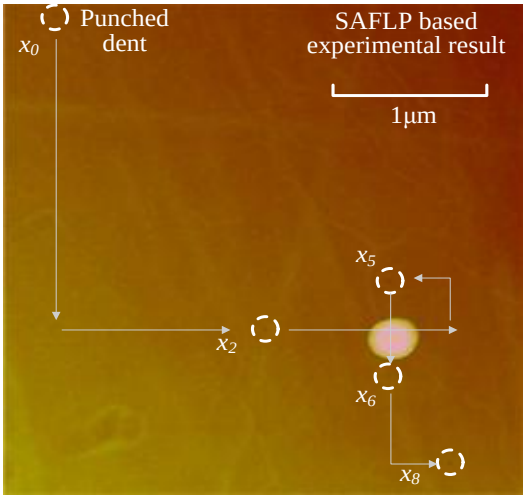

Fig.11. The tip is moved from x_0 to x_8 by using the SAFLP based algorithm. The tip positions at x_0, x_8 and the waypoints are recorded by punching the dents. Scanning image shows that these punched dents observed in the white dash line circles marks the tip positions in the different way points. 50 experiments have been performed.

Fig.12 (a) and (b) plot the tip position data recorded by the dents punched on substrates in two kind experiments. Fig.13 and Fig.14 show and contrast experimental results in 3D histogram, and the Gaussian fitted curves for the distributions in *X* and *Y* directions at start position x_0 and target position x_8. Especially according to histogram results (see Fig.13 (b) and Fig.14 (b)), the uncertainty distribution of the tip position is significantly reduced by SAFLP based method.

Table 1. Simulation and experimental results based on direct move without applying SAFLP algorithm. (μm)

	Simulation data				Experimental data			
	μ_x	μ_y	σ_x	σ_y	μ_x	μ_y	σ_x	σ_y
x_0	−1.245	1.316	0.013	0.016	−1.333	1.435	0.014	0.018
x_{d_1}	−1.245	−1.381	0.013	0.021	−1.346	−1.324	0.014	0.024
x_8	1.031	−1.434	0.018	0.021	1.087	−1.374	0.021	0.025

Table 2. Simulation and experimental results based on local scan with SAFLP algorithm. (μm)

	Simulation data				Experimental data			
	μ_x	μ_y	σ_x	σ_y	μ_x	μ_y	σ_x	σ_y
x_0	−1.245	1.316	0.013	0.016	−1.319	1.474	0.015	0.019
x_1	−1.245	−0.645	0.013	0.020				
x_2	0.239	−0.700	0.016	0.020	−0.009	−0.599	0.017	0.022
x_{3_kp}	0.802	−0.701	0.006	0.020				
x_3	1.220	−0.701	0.006	0.020				
x_4	1.255	−0.407	0.006	0.020				
x_5	0.804	−0.371	0.008	0.020	0.792		0.006	
x_{6_kp}	0.771	−0.682	0.008	0.006				
x_6	0.764	−0.985	0.008	0.006	0.783		0.010	
x_7	0.761	−1.431	0.008	0.008				
x_8	1.101	−1.471	0.009	0.008	1.178	−1.495	0.010	0.007

Note: the empty cells in the table mean that there is no punching dent or the tip performs no positioning on *y* direction

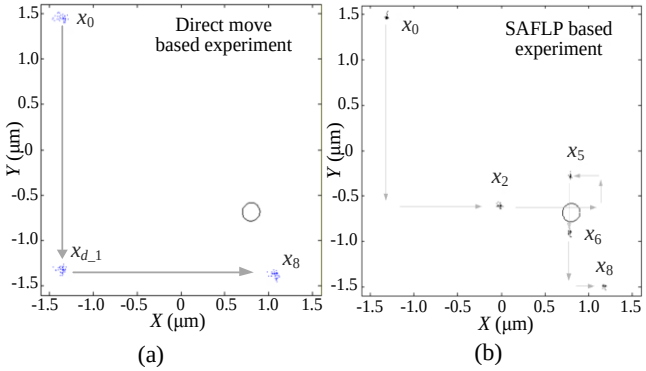

Fig.12. (a) Experiment Result: Tip distributions of direct move based experiment (50 experiments). (b) Experiment Result: Tip distributions of the SAFLP based experiment (50 experiments).

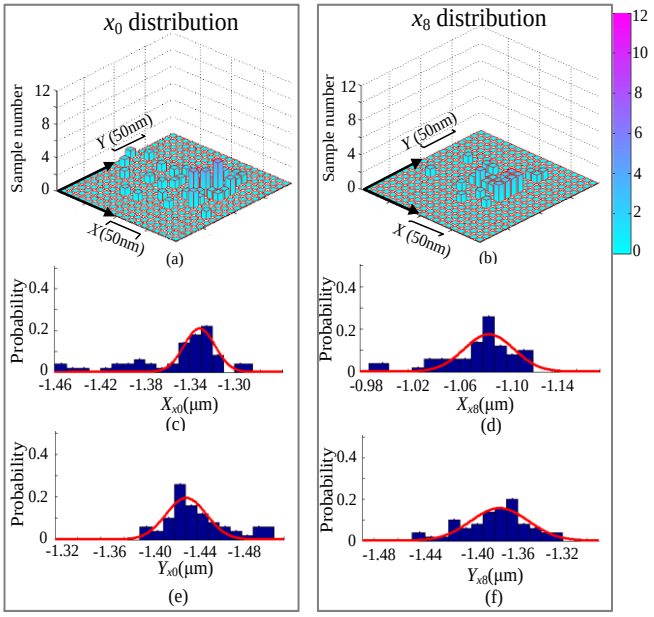

Fig.13. Gaussian fitted results for the tip distribution at x_0 and x_8 in direct moving experiment. (a) and (b) are the tip distributions zoomed in at x_0 and x_8. (c) and (d) are the fitted curves for the distributions in *x* and *y* directions at x_0, respectively. (e) and (f) are the fitted curves for the distributions in *x* and *y* directions at x_8, respectively.

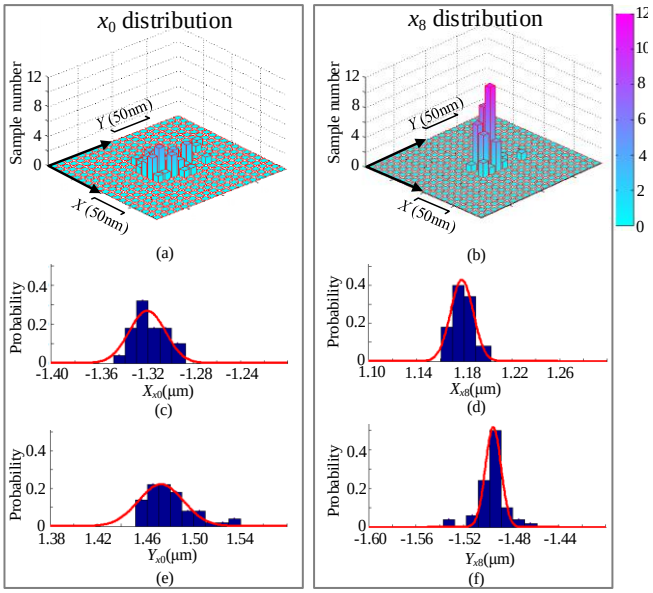

Fig.14. Gaussian fitted results for the tip distribution at x_0 and x_8 in local scan based moving. (a) and (b) are the distributions zoomed in at x_0 and x_8. (c) and (d) are the fitted curves for the distributions in *x* and *y* directions at x_0, respectively. (e) and (f) are the fitted curves for the distributions in *x* and *y* directions at x_8, respectively.

V. Evaluation on Positioning Accuracy

A. Positioning Accuracy

In SAFLP approach, high accuracy of tip positioning will be realized by following three strategies. The first is incorporating a motion model with higher accuracy that is depending on both performance of the AFM itself and the modeling quality including calibration accuracy. The second one is building high accuracy feature map and observation model that is the most essential to position estimation updating. The positioning accuracy just after the observation could be significantly improved to the level near to the observation accuracy, even for the prior tip position with relatively large uncertainty. The third strategy is to keep short moving distance after the local scan based feature observation and position updating, since long distance motion will lead bigger uncertainty of the tip position. This can be realized by choosing a feature that is near enough to the target position of manipulation task.

B. Experiment on High Accurate Tip Position Estimation

An experiment is performed for demonstrating the high accurate tip position estimation by using the local scan based feature observation and tip position updating. A carbon nano-tube (see Fig.15(a)) is selected as the feature of

one-direction local scan by using the accurate map and motion model described in this session.

Not only for convenience on obtaining zoom-in rescan image of experiment results, but also for having the relatively constant initial tip distribution within the same experiment, we designed an experiment plan shown in Fig.15(b). The tip initially starts from position x_0. It scans up first to position x_1, then scans down to position x_2, then x_3, the target position without horizontal motion, and punches a dent on the substrate. The scanning up motion is with a fixed distance of 500nm, and the relative position to the scanned point of the nano-tube has been estimated by using the local scan based observation. Based on the estimated position x_1, the tip motion is planned to move to the position x_2 that is 50nm away from the center of the nano-tube. In this moving-down, the tip position updating has been performed again. Based on this updated position, the tip is moved to position x_3 where is 130nm away from position $x_{2,kp}$, the center of the scanned nano-tube. After punching a dent to record the tip position, the tip moved a certain distance horizontally and repeat the abovementioned x_0-x_1-x_3 vertical loop motion with local scans. In this experiment, we repeated this motion 6 times.

(a) The carbon nano-tube as the features and 6 dents punched

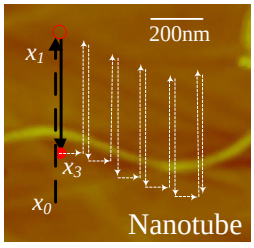

(b) Path of the tip motion

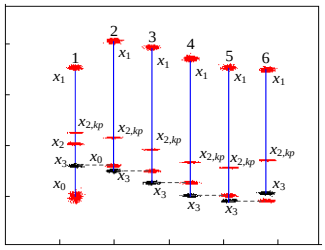

(c) Calculated tip position and distribution

Fig.15. Experiment setting, scanning path, and calculated tip position and distribution. (a) The carbon nano-tube used as the feature for tip positioning, and 6 dents punched under the nano-tube as the tip positioning results. (b) The experiment consists of 6 scanning and positioning experiment sub-paths which are stopped at 130nm away from the nano-tube. (c) Numerical calculation results of tip position and distribution in 6 experiments.

Fig.15 (c) is the simulation result of the position distribution of the AFM tip in waypoints of 6 up-and-down scanning motions. Fig.16 is the experiment result and statistic data of the distance from the punched dent to the center position of the carbon-nano tube where the tip has scanned over. The error of the distance mean value is 0.4nm and the maximum error from the target distance is 2.2nm.

From the results, it is easy to know that in the meaningful accuracy, 1 digit of the sub-nm order, there is no difference among three cases on standard deviation of the tip position distribution. When checking the results of the 1 digits under the sub-nm order, there are some small differences at the position x_1 after the first scanning and updating, but no difference can be observed at position x_2, and at the target position x_3 after the second scan and updating. Of course, the difference at 1 digits under sub-nm is not really necessary to be cared. These results indicated that after two scanning and updating motions, there is no difference in the positioning results of the AFM tip even with different initial distribution of the tip. Based on this, we only focus the vertical distance between the nano-tube center position and the punched dents, and discuss the tip position accuracy by counting 6 up-and-down scanning results statistically. The results shown in Fig.16 and Table 3 illustrate that tip position distribution in experiments is in the same order and smaller than the distribution obtained from the numerical calculation. This result illustrates that the proposed SALFP based algorithm is able to be used for planning the tip motion during nano-manipulations.

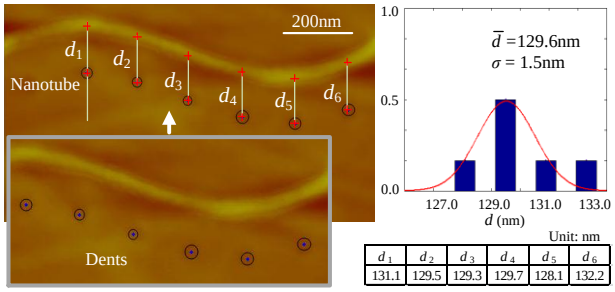

d_1	d_2	d_3	d_4	d_5	d_6
131.1	129.5	129.3	129.7	128.1	132.2

Fig.16. Experiment results and their statistic evaluation of 6 scanning and positioning motions recorded by dents punched at the position of 130nm from the nano-tube.

Table 3. Simulation results of tip positioning in three cases with different initial position distribution of the AFM tip. (nm)

	Case 1 (σ_{y_0}=20)		*Case* 2 (σ_{y_0}=15)		*Case* 3 (σ_{y_0}=5)	
	u_y	σ_y	u_y	σ_y	u_y	σ_y
x_0	0.0	20.0	0.0	15.0	0.0	5.0
x_1	507.5	3.7	507.4	3.7	507.2	3.7
$x_{2,kp}$	251.5	1.2	251.5	1.2	251.5	1.2
x_2	208.2	1.9	208.2	1.9	208.2	1.9
x_3	122.0	2.8	122.0	2.8	122.0	2.8

VI. CONCLUSIONS

The tip position uncertainties in the AFM based nano-manipulation exist due to the thermal drift, the nonlinearity of the AFM scanner and other error sources. This study proposes a stochastic approach for feature-based localization and plan in nano-manipulations. The spatial uncertainties of the tip position are first described by probability distribution at nano-scale. For reducing the spatial uncertainties, the feature is intermittently perceived to stochastically estimate the tip distribution by local scan based observation. At the same time, the tip motion model is first statistically built by integrating the PI model, the creep model and the thermal drift model, and used to combine with the observation model for optimally updating the tip position by using the Kalman filter. Furthermore, for calibrating the probabilistic parameters of the observation model and motion model, several experiments are designed and performed. Finally, the simulation and corresponding experiments are carried out to illustrate the validity of the calibrated parameters and the SAFLP based algorithm. The experimental results demonstrate that the stochastic approach successively applied

in macro-robotics can also be appropriate for nano-robotics, because the uncertainties in the nano-environment have more influence on manipulation, and are very difficult to be clearly clarified and accurately modeled.

As for the unpredictable nano-environment, high accurate positioning method with long term stabilization is a key technology to achieve nano-manipulation. In the long run, novel nano-devices and nano-structures will be developed with higher precision and even massively fabricated with an automatic way to increase the manufacture efficiency. The proposed method, with reducing the tip uncertainties caused by thermal drift, PZT nonlinearity and other errors sources, lays the foundation for long term automated manufacture strategy, and will extend its range of applications in the future.

ACKNOWLEDGMENT

This research work is supported by the National Natural Science Foundation of China (Project Codes: 61175103, 61305125), National Post Doctor Foundation (Project Codes: 2013M530955, 2014T70265), The National 863 project (2012AA020100) and Chinese Academy of Sciences State Foreign Expert Bureau International Partnership Program for Creative Research Teams.

REFERENCES

[1] B. Bhushan, Springer Handbook of Nano-technology, Springer press, New York, 2005, pp.638-648.

[2] N. Xi and W.J. Li, "Editorial Recent Development in Nanoscale Manipulation and Assembly," *IEEE T. Robot. Atom.*, vol. 3, no. 3, pp. 194-198, 2006.

[3] S. Fatikow, "Trends in Nanohandling Automated Nanohandling by Microrobots," Springer Series in Advanced Manufacturing, Springer press, London, 2008, pp.1-22.

[4] C.D. Onal, O. Ozcan, and M. Sitti, "Automated 2-D Nanoparticle Manipulation Using Atomic Force Microscopy," *IEEE T. Nanotechnol.*, vol. 10, no. 3, pp. 472-481, 2011.

[5] C. Onal and M. Sitti, "Teleoperated 3D Force Feedback from the Nanoscale with an Atomic Force Microscope," *IEEE T. Nanotechnol.*, vol. 9, no. 1, pp. 46-54, Jan. 2010.

[6] H. Xie, C. Onal, S. Régnier, M. Sitti, "Force microscopy based nanorobotics: modeling, simulation, setup building and experiments, Springer-Verla, ISBN 978-3-642-20328-2, 2011,pp.13-26

[7] M. Sitti and H. Hashimoto, "Controlled pushing of nanoparticles: modeling and experiments," *IEEE-ASME T. Mech*., vol. 5, no. 2, pp. 199-211, 2000.

[8] S. Decossas, F. Mazen, T. Baron, G. Bremond, and A.Souifi, "Atomic force microscopy nanomanipulation of silicon nanocrystals for nanodevice fabrication," *Nanotechnology*., vol. 14, no. 12, pp. 1272-1278, 2003.

[9] G.X. Li,W.X. Wang,Y.C. Wang, S. Yuan,W.G.Yang,N.Xi,L.Q. Liu, "Nano-Manipulation Based on Real-Time Compressive Tracking" *IEEE T. Nanotechnol.*,vol.14, no.5, pp.837 - 846, 2015.

[10] H.P. Chen,N. Xi, and G.Y. Li, "CAD-guided automated nanoassembly using atomic force microscopy-based nonrobotics," *IEEE T. Robot. Atom.*, vol. 3, no. 3, pp. 208-217, 2006.

[11] B. Mokaberi and A. A. G. Requicha, "Compensation of Scanner Creep and Hysteresis for AFM Nanomanipulation," *IEEE T. Autom. Sci. Eng.*, vol. 5, no. 2, pp. 197-206, 2008.

[12] F. Krohs, C. Onal, M. Sitti, and S. Fatikow, "Towards Automated Nanoassembly With the Atomic Force Microscope: A Versatile Drift Compensation Procedure," *J. Dyn. Syst. Meas. Contr.*, vol. 131, no.3, pp. 061106-061113, 2009.

[13] Y. Wu, and Q.Z. Zou, "Iterative Control Approach to Compensate for Both the Hysteresis and the Dynamics Effects of Piezo Actuators," *IEEE T. Contr. Syst. T.*, vol. 15, p. 936-944,2007.

[14] U. X. Tan, W. T. Latt, C. Y. Shee, C. N. Riviere, W. T. Ang, "Feedforward Controller of Ill-Conditioned Hysteresis Using Singularity-Free Prandtl–Ishlinskii Model," *IEEE-ASME T. Mech.*, vol. 14, p. 598-605, 2009.

[15] J. T. Woodward and D. K. Schwartz, "Removing drift from scanning probe microscope images of periodic samples," *J. Vac. Sci. Technol*. B, vol. 16, no. 1 pp. 51-53, 1998.

[16] B. Mokaberi and A.A.G. Requicha, "Drift compensation for automatic nanomanipulation with scanning probe microscopes," *IEEE T. Autom. Sci. Eng.*, vol. 3, no. 3, pp. 199-207, 2006.

[17] Q.M. Yang, S. Jagannathan, E.W. Bohannan, "Automatic Drift Compensation Using Phase Correlation Method for Nanomanipulation," *IEEE T. Nanotechnol*, vol. 7, pp. 209-216, 2008.

[18] S. Thrun, W. Burgad, and D. Fox, Probabilistic Robotics. London, England: The MIT Press, Cambridge, Massachusetts, 2005,pp.4-8.

[19] L.Q. Liu, N. Xi, Y.C. Wang, Z.L. Dong, and U.C. Wejinya, "Landmark based sensing and positioning in robotic nano manipulation," in *Conf. IEEE ROBIO*, 2008, pp. 37-42.

[20] S. Thrun, "Probabilistic Robotics," Commun. ACM, vol. 45,no. 3, pp. 52-57, 2002.

[21] J. J. Leonard and H. F. Durrant-Whyte, "Mobile robot localization by tracking geometric beacons," *IEEE T. Robot. Atom*., vol. 7, no. 3, pp. 376-382, 1991.

[22] S. Yuan, L.Q. Liu, Z.D. Wang, N. Xi, Y.C. Wang, Z.L. Dong, and Z.Y. Wang, "A probabilistic approach for on-line positioning in nano manipulations,"in *Conf. IEEE WCICA*, 2010, pp. 450-455.

[23] S. Yuan, L.Q. Liu, Z.D. Wang, N. Xi, Y.C. Wang, Z.L. Dong, and Z.Y. Wang,"A Probability Approach for On-line Tip Localization with Local Scan Based Landmark Sensing in Nanomanipulations," in Conf. 3M-NANO 2011,China pp.1-6.

[24] H. Xie, and S. Régnier, "High-efficiency automated nano-manipulation with parallel imaging/manipulation force microscopy," *IEEE T. Nanotechnol*, vol. 11, no. 1, 21–32, 2012.

[25] H. Xie, and S. Régnier, "Development of a flexible robotic system for multiscale applications of micro/nanoscale manipulation and assembly," *IEEE-ASME T. Mech*., vol. 16, no. 2, pp.266–276, 2011.

[26] G.Y Li, N. Xi, H.P. Chen, C.A. Pomeroy and M. Prokos, "Videolized" atomic force microscopy for interactive nanomanipulation and nanoassembly," *IEEE T. Nanotechnol.*, vol. 4, no. 5, pp. 605-615, 2005.

[27] J.B. Zhang, N. Xi, G.Y. Li, C. Ho-Yin, and U.C. Wejinya, "Adaptable End Effector for Atomic Force Microscopy Based Nanomanipulation," *IEEE T. Nanotechnol.*, vol. 5, no. 6, pp. 628-642, 2006.

[28] W. Vogl, M. Bernice Kai-Lam, and M. Sitti, "Augmented reality user interface for an atomic force microscope-based nanorobotic system," *IEEE T. Nanotechnol*., vol. 5, no. 4, pp. 397-406, 2006.

[29] G. Li, N. Xi, M. Yu, and W. Feng, "Development of augmented reality system for AFM-based nanomanipulation," *IEEE-ASME T. Mech*., vol. 9, no. 2, pp. 358-365, 2004.

[30] L.Q. Liu, Y.L. Luo, N. Xi, Y.C. Wang, J.B. Zhang, and G.Y. Li, "Sensor Referenced Real-Time Videolization of Atomic Force Microscopy for Nanomanipulations," *IEEE-ASME T. Mech.*, vol. 13, no. 1, pp. 76-85, 2008.

[31] J. Hou, L.Q. Liu, Z.Y. Wang, Z.D. Wang, N. Xi, Y.C. Wang, *et al.*, "AFM-Based Robotic Nano-Hand for Stable Manipulation at Nanoscale," *IEEE T. Autom. Sci. Eng*., vol. 10, pp. 285-295, 2013.